Chapter 3
The Effect of Mechanical Load-induced Intraosseous Pressure Gradients on Bone Remodeling

Emilio Barchiesi, Ivan Giorgio, Faris Alzahrani & Tasawar Hayat

Abstract It is well established that changes in bone blood and interstitial fluid flows are associated with changes in the bone remodeling process. These flows in bone are a result not only of trans-cortical pressure gradients produced by vascular and hydro-static pressure, but also of mechanical loadings. Mechanical load-induced intraosseous pressure gradients may result in some fluid stimuli effects which, in turn, may enable bone cells to detect external mechanical signals. In this paper, the exploitation of a 2D continuum model based on classical poroelasticity is presented within a variational framework. The investigation is aimed at describing how mechanical actions can affect the remodeling process of a bone tissue. The focus is on the introduction of a physically motivated strain energy contribution aimed to take into account the presence of saturating fluid in the interconnected pores of bone tissue. The interaction with a bio-resorbable organic ceramic material like those used in bone graft implants is also considered in presented model. Numerical results are provided in a relevant exemplary case.

Keywords: Mechanical–biological coupling · Bone functional adaptation · Growth resorption processes · Bone remodeling

Emilio Barchiesi & Ivan Giorgio
Department of Structural and Geotechnical Engineering, Università degli studi di Roma La Sapienza, 18 Via Eudossiana, Rome & International Research Center for the Mathematics and Mechanics of Complex Systems - MeMoCS, Università degli studi dell'Aquila, L'Aquila, Italy,
e-mail: BarchiesiEmilio@gmail.com, ivan.giorgio@uniroma1.it

Faris Alzahrani
NAAM Research Group, Department of Mathematics, King Abdulaziz University, Jeddah 21589, Saudi Arabia,
e-mail: faris.kau@hotmail.com

Tasawar Hayat
Department of Mathematics, Quaid-I-Azam University, Islamabad, Pakistan & NAAM Research Group, Department of Mathematics, King Abdulaziz University, Jeddah 21589, Saudi Arabia,
e-mail: pensy_t@yahoo.com

B. E. Abali et al. (eds.), *New Achievements in Continuum Mechanics and Thermodynamics*, Advanced Structured Materials 108,
https://doi.org/10.1007/978-3-030-13307-8_3

3.1 Introduction

In bone tissue, it is possible to distinguish mainly two kinds of fluids: blood and interstitial fluids like, e.g., bone marrow. Blood carries through the arterial system oxygen and other nutrients, and the blood components depart from this arterial system via smaller channels, i.e. the venous system, to zones containing less oxygen and reduced nutrition (see, e.g., George et al, 2018a; Spingarn et al, 2018). Within the bone, as within other tissues, substances pass from the blood flowing through the arterial walls into the interstitial fluid. The interstitial fluid subsequently carries these substances to the cells within the bone and, at the same time, carries away the waste materials from the cells. Bone tissue would not remain alive without these fluid movements. It is thus clear the reason why it is commonly accepted that vascularization is required for effective bone healing and maintenance. These statements are supported by the fact that changes in bone blood and interstitial fluid flows are associated with changes in bone remodeling and formation (see, e.g., Hillsley and Frangos, 1994). These flows in bone are a result not only of trans-cortical pressure gradients produced by vascular and hydro-static pressure, but are also related to externally applied mechanical loadings. It is observed that flow rates are affected by many factors, like the increase in venous pressure due to hypertension, the fluid shifts occurring in bedrest or microgravity, the increase in vascularization during the injury-healing response, and the mechanical compression/tension and bending/torsion of bone during exercise. Thus, mechanical load-induced intraosseous pressure gradients, like those induced by mechanical loading of bone during exercise, affect the fluid flow rate and, eventually, bone remodeling. The purpose of this article is to present a mathematical model able to describe the role of mechanical actions in the bone osteogenesis process. In this paper we will make use of the classical poroelasticity theory, as formulated by Biot in its 1941's foundational paper (Biot, 1941), suitably complemented with a novel non-local energy contribution purposely introduced to account for fluid compression. In poroelasticity, a field accounting for porosity is usually introduced in addition to the placement function of the solid phase. Poroelasticity is, thus, a so-called micromorphic theory, belonging to the wider class of generalized continua with internal variables or with extra kinematical descriptors. The importance of these continua has been questioned, but, in our opinion, has been proven useful in presence of long range interactions at micro-level, when a macro continuous model is more suitable (see, e.g., Alibert et al, 2003; Eremeyev et al, 2018a; Abali et al, 2017; Pietraszkiewicz and Eremeyev, 2009). The macroscopic theories formulated in the framework of the mechanics of generalized continua is being formulated for 3D and 2D bodies and is increasingly attracting the attention of those researchers interested in non-standard mechanical effects (see, e.g., Altenbach and Eremeyev, 2009; Bertram and Glüge, 2016; Gusev and Lurie, 2017; Camar-Eddine and Seppecher, 2001). The recent literature stresses two aspects of the considered multi-scale mechanical systems: their potentially exotic macroscopic behavior and the corresponding microscopic structure, in which there are eventually active long range interactions. The need for generalized continua, including in this class also higher gradient theories (dell'Isola and

Seppecher, 1997; dell'Isola et al, 2012; dell'Isola and Steigmann, 2015; dell'Isola et al, 2016, 2015b), is unavoidable when one has to describe those mechanical phenomena which involves the activation of deformation modes at microlevel determining the interaction of parts of the micro-structure having high stiffness contrast and bridging distant homogenization cells. These complex deformation patterns cannot be accounted for in standard Cauchy theories: for a series of examples of this circumstance, see e.g., Cuomo et al (2016); dell'Isola et al (2016); Placidi et al (2016) while for theoretical arguments dealing with micro-macro convergence motivating higher gradient theories, see e.g., Abdoul-Anziz and Seppecher (2018); Seppecher et al (2011); Pideri and Seppecher (1997). In the present paper, we deal with a reconstructed bone during its remodeling process. This is surely a multi scale complex system, which involves mechanical, chemical and biological aspects and, therefore the previous modeling concerns are surely appropriate. This approach is present in the literature of biomechanics of bones (see, e.g., Lekszycki and dell'Isola, 2012; Giorgio et al, 2017; Ganghoffer, 2016; Goda et al, 2014, 2012; Ganghoffer, 2012) but has attracted the attention also in view of different possible applications. Generalized continua are indeed considered also for modeling electromechanical systems in biological applications (see, e.g., Steigmann and Agrawal, 2016) memory shape alloys (Shirani et al, 2017) and piezo/flexo-electric materials (see, e.g., Abdalladan et al, 2017; Abd-alla et al, 2017; Pagnini and Piccardo, 2016; Enakoutsa et al, 2017). These studies may have a relevance in the process of bone remodeling, if one of the mechanisms regulating considered bone growth process are regulated by electromagnetically induced biological activity, as it seems to happen when electrical currents are used to favor bone growth. Growing bones are resisting to external load, also in elastic regime: therefore, generalized elastic continua can be of use in the class of biomechanics phenomena which we consider here. In this context, the works (Andreaus et al, 2010; Rosi et al, 2018; Abali et al, 2015; Altenbach and Eremeyev, 2015; Franciosi et al, 2018; Spagnuolo and Andreaus, 2018; Andreaus et al, 2018), which try to capture some aspects of the elastic deformation of reconstructed bones, are relevant. As we hope to have explained already in an exhaustive way, the complexity of behavior of a reconstructed bone does not allow for too drastic simplifications. Surely in the small and larger channels in which interstitial fluids are flowing may activate capillary phenomena: therefore, the analysis of capillary fluids (Auffray et al, 2015; Seppecher, 1993, 2000) and their influence at macro-level may be of relevance. In this context, the results presented in Madeo et al (2013); Sciarra et al (2007) may be of use, as well as the analysis of damage phenomena (see, e.g., Placidi et al, 2018; Rinaldi and Placidi, 2014; Placidi, 2015; Misra and Singh, 2013; Spagnuolo et al, 2017; Goda and Ganghoffer, 2015; Di Nino et al, 2017; Battista et al, 2017b) based on generalized continuum models. Remark that in the last paper a purely discrete model for mechanical phenomena is introduced, based on the postulation involving a generalization of cellular automata. Indeed, among the other feed-back mechanisms which regulate bone remodeling, it has been proven that it is particularly effective that which activates the action of osteoblasts and osteoclast when the microstructure of the bone exhibits some growing damage and micro fracture. One should not, however, believe that the only feed-back control

mechanism of growth involves a measure of micro-fracture of bone. It seems that also the dissipation occurring in the interstitial fluids at the level of micro-canalicula and micro-trabecular structure may be effective. As a consequence dissipation phenomena has to be included in the modeling process (e.g. using the ideas presented in Lekszycki et al (2017); Cuomo (2017); Luongo and D'Annibale (2017). If the considered phenomena involve lower scales then the granular structure of the bone and the reconstructing material must be accounted for: in this case the modeling issues addressed in Misra and Poorsolhjouy (2015a); Misra and Singh (2015); Misra and Poorsolhjouy (2015b); Altenbach et al (2010); Eremeyev (2018), may become relevant. Finally, it has to be remarked that the peculiar features exhibited by reconstructed bones and by physiological bones imply some specific corresponding nonstandard characteristics in wave propagation. These peculiarities may be exploited to get informations, using noninvasive methods, about the health and mechanical performance of (possibly reconstructed) bone tissue. In this case wave propagation analysis proposed in Placidi et al (2008); Engelbrecht and Berezovski (2015); Berezovski et al (2018); Abbas et al (2016); Eremeyev et al (2018b) while dynamic analyses performed in Battista et al (2015, 2017a); Ferretti et al (2017) may be of use.

The plan of the work present is the following: first, in Sect. 3.2, we address some basic facts on bone physiology, and will extrapolate the main information needed for the modeling. Then, in Sect. 3.3, we introduce the proposed continuum model. The focus is on the introduction of a physically motivated dedicated strain energy contribution due to the presence of saturating fluid in the interconnected pores of bone tissue and the interaction with a bio-resorbable organic ceramic material like those used in bone graft implants is considered. In Sect. 3.4, we provide numerical results in a relevant exemplary case. Finally, in Sect. 3.5, we give conclusions and perspectives.

3.2 Some Considerations on Bone Physiology

Bone is a 'rigid' living organ that constitutes the vertebrate skeleton; it protects the organs of the body and enables mobility. It has a honeycomb-like matrix internally, which helps to give the bone rigidity and that can be considered porous with respect to the characteristic length that we are concerned with at the macroscopic level. The pores of the solid matrix are filled with interstitial fluid. Inside bone tissue, different types of bone cells act. Osteoblasts and Osteocytes are involved in the formation and mineralization of bone; Osteoclasts are involved in the resorption of bone tissue. Modified (flattened) Osteoblasts become the lining cells that form a protective layer on the bone surface. The mineralized matrix of bone tissue has an organic component of mainly collagen, called ossein, and an inorganic component of bone mineral made up of various salts. Bone tissue is a mineralized tissue of two types, cortical and cancellous bone. Other types of tissue found in bones include bone marrow, endosteum, periosteum, nerves, blood vessels and cartilage. Bone tissue is con-

stantly reshaped by the biological activity which takes place therein. Biology tells us that the basic (feedback) mechanism, relevant for the subsequent modeling, is the one shown in Fig. 3.1. External mechanical actions are sensed by the Osteocytes which, being actors of the mechano-transduction process, transduce the mechanical stimulus into a biological, i.e. bio-chemical, signal, inducing the resorption of bone tissue by the Osteoclasts or its synthesis by the Osteoblasts. Bio-resorbable artificial materials can be roughly divided into polymeric and ceramic materials. Polymers are mainly degraded in the process of hydrolysis, while organic ceramics like, e.g., β-TCP (Tri-Calcium Phosphate) with 5% of HAP (Hydroxyapatite), are instead mostly processed by the Osteoclasts. Both processes always coexist and, depending on the constitution of the graft, one process or the other results to be dominant. In this paper we consider resorption due to Osteoclasts only. Taking into account the presence of a bone graft allows to better understand and predict how mechanical actions can affect the remodeling process of a bone tissue possibly interacting with a bio-resorbable material like those used in bone graft implants (e.g. dental bone grafting), whether the implanted graft is suitable as mechanically supporting element, the capability of the graft to integrate with the bone tissue, so that it can be gradually resorbed and replaced by new natural bone tissue. This last property is conferred by chemical composition, number and size of pores, because they determine the extent to which living cells migration, their expected activities, the development of vascularization for cell survival etc. can occur.

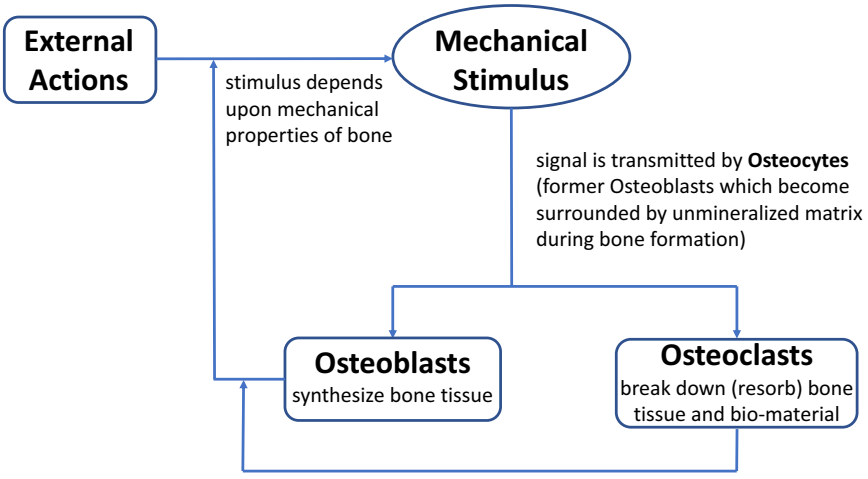

Fig. 3.1 Basic feedback mechanism in a bone. A detailed description of the physiology of bone remodeling would be out of reach.

3.3 Modelling

3.3.1 Kinematics

In this paper we are aimed only at showing the main features of the model and, thus, notwithstanding the fact that the subsequent modeling is suitable also for the study of 3D bodies, it is here sufficient to consider a 2D body. Such a body is made up of a mixture composed by three phases: the binary solid porous matrix of bone (B) and bio-resorbable graft material (M) and the fluid phase (F) that fills the connected pores of the solid matrix. The shape of the body in its undeformed reference configuration is represented by the subset $\mathcal{B}_0 \subset \mathbb{R}^2$. We will not make use of a so-called mixture model in a strict sense, meaning that we are not going to consider as independent kinematical descriptors of the model placement functions for each component of the mixture. The only (sufficiently regular) displacement field $u : \mathbb{R}^2 \supseteq \mathcal{B}_0 \to \mathbb{R}^2$, with $\chi(X) = X + u(X)$ being the corresponding placement function, which we consider as an independent Lagrangian kinematic variable is such that $u(X, t)$ is the displacement of the solid binary mixture in the representative three-phase volume element (see Fig. 3.2) whose barycenter is in X in the reference configuration.

While the relative displacement of the components of the solid matrix can be neglected, the same does not hold for the fluid phase, which in general can move (only, as impermeability of the solid matrix is here assumed) inside the solid matrix. The set $\mathcal{B} \equiv \chi(\mathcal{B}_0) \subset \mathbb{R}^2$ is the current shape of the body. We shall denote the Lagrangian representation $e\left(\chi(X)\right)$ of an Eulerian field $e(x)$, where $x \in \mathcal{B}$ and it

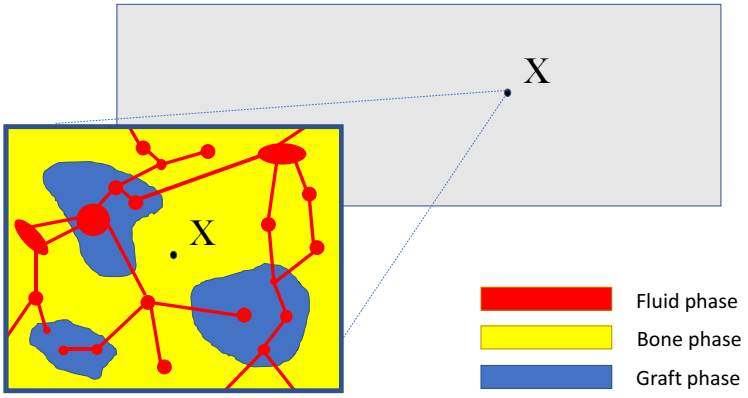

Fig. 3.2 A rectangular 2D body with a zoomed schematic of a representative volume element (RVE).

is such that $x = \chi(X)$, with $e^{\mathcal{L}}(X)$. The (apparent) Lagrangian mass density in the reference configuration $\rho_R(X)$, with $X \in \mathcal{B}_0$, is given by

$$\rho_R(X) = \sum_{i=B,M,F} \rho_{i,R}(X) = \sum_{i=B,M,F} \hat{\rho}_{i,R}(X)\xi_{i,R}(X), \tag{3.1}$$

where $\rho_{i,R}$ is the partial Lagrangian mass of component i in the mixture in the reference configuration, is the $\hat{\rho}_{i,R}$ (true) Lagrangian mass density of component i in a mono-phase mixture in the reference configuration, $\xi_{i,R}$ is the Lagrangian volume fraction of component i in the mixture in the reference configuration which, since the porous solid matrix is saturated with fluid, is also referred to as the porosity in the reference configuration. The (apparent) Eulerian mass density in the current configuration $\rho_C(x)$, $x \in \mathcal{B}$, is given by

$$\rho_C(x) = \sum_{i=B,M,F} \rho_{i,C}(x) = \sum_{i=B,M,F} \hat{\rho}_{i,C}(x)\xi_{i,C}(x), \tag{3.2}$$

with $\rho_{i,C}$ the partial Eulerian mass of component i in the mixture in the current configuration, $\hat{\rho}_{i,C}$ the (true) Eulerian mass density of component i in a mono-phase mixture in the current configuration, $\xi_{i,C}$ the Eulerian volume fraction of component i in the mixture in the current configuration which, since the porous solid matrix is saturated with fluid, is also referred to as the porosity in the current configuration (Wilmanski, 1998). As we mentioned above, in this paper we consider undrained conditions, i.e. impermeability conditions at the boundary. Thus, the following global (as opposed to local) mass conservation constraint holds for the fluid phase

$$\int_{\mathcal{B}_0} \rho^{\mathcal{L}}_{F,C}(X)\ \mathrm{det}\nabla\chi \mathrm{d}X = \int_{\mathcal{B}_0} \rho_{F,C}\left(\chi(X)\right)\ \mathrm{det}\nabla\chi \mathrm{d}X \tag{3.3}$$

$$\int_{\mathcal{B}} \rho_{F,C}(x)\ \mathrm{d}x = M_F = \int_{\mathcal{B}_0} \rho_{F,R}(X)\ \mathrm{d}X, \tag{3.4}$$

with M_F being the total fluid mass in the body. Finally, in the spirit of continuum poroelasticity, we introduce another independent Lagrangian micromorphic field $\vartheta : \mathbb{R}^2 \supseteq \mathcal{B}_0 \to \mathbb{R}$, which is the change of porosity. Following Coussy (2004), we assume that

$$\vartheta(X) \coloneqq \xi_{F,C}\left(\chi(X)\right) - \xi_{F,R}(X) = \xi^{\mathcal{L}}_{F,C}(X) - \xi_{F,R}(X). \tag{3.5}$$

3.3.2 Elastic Mechanical Energy Stored Within the Body

For fixed $\xi_{B,R}$, $\xi_{M,R}$ (remind that $\xi_{F,R} = 1 - \xi_{B,R} - \xi_{M,R}$), the system is assumed to behave elastically. We consider the quasi-static case, i.e. inertia and micro-inertia forces/energies are negligible, and the total deformation energy of the system is

assumed to be

$$\psi = \psi_{\text{STRAIN}} - \psi_{\text{EXT}} \tag{3.6}$$

with

$$\psi_{\text{STRAIN}} = \psi_{\text{POR}} + \psi_{\text{PERIDYN}} \tag{3.7}$$

and

$$\psi_{\text{EXT}} = \int_{\mathcal{B}_0} b^{ext} \cdot u \, \mathrm{d}X + \int_{\partial\mathcal{B}_0} f^{ext} \cdot u \, \mathrm{d}X, \tag{3.8}$$

the quantities b^{ext} and f^{ext} in (3.8) being, respectively, bulk and surface loads (see for more detail on variational formulation e.g. Abali et al, 2017; Eugster and Glocker, 2017). Let us now examine the terms ψ_{POR} in (3.7), which is the poro-elasticity strain energy density contribution in Lagrangian form i.e. the energy stored within the body due to the deformation of the solid matrix and to pores surface tension and related phenomena (Giorgio et al, 2016). In this paper we consider the small strain assumption (i.e. $\nabla u \simeq 0$) and, in what follows, $E = \text{Sym}\nabla u$ is the linearized Green-Saint Venant strain tensor. The purely (no pre-stress) quadratic form in the strain E and micro-strain ϑ is

$$\psi_{\text{POR}}(E,\vartheta) = \int_{\mathcal{B}_0} \Bigg[\underbrace{\frac{Q}{2}\left(\vartheta - \alpha\,\text{tr}(E)\right)^2}_{\text{Biot's contribution}} + \underbrace{\frac{1}{2}\frac{Y(\rho_{B,R},\rho_{M,R})\nu}{(1-2\nu)(1+\nu)}\text{tr}(E)^2 + \frac{1}{2}\frac{Y(\rho_{B,R},\rho_{M,R})}{(1+\nu)}\text{tr}(E^2)}_{\text{isotropic strain energy density of the solid bone+graft mixture}} \Bigg] \mathrm{d}X \tag{3.9}$$

where

$$Y = Y_B \xi_{B,R}^{\beta_B} + Y_M \xi_{M,R}^{\beta_M} \tag{3.10}$$

is the effective bone-graft Young modulus, Y_B is the bone Young modulus, Y_M is the graft Young modulus, β_B and β_M are two constitutive exponents, ν is the effective bone-graft Poisson's ratio (set to be 0.3), $Q > 0$ is the 1^{st} Biot parameter (resistance to change of porosity), and α is the 2^{nd} Biot parameter. Specifically, for the sake of simplicity, we set

$$\alpha = \frac{Y}{H_1\, 3(1-2\nu)} \qquad \frac{1}{Q} = \frac{1}{R} - \frac{\alpha}{H_1} \tag{3.11}$$

with H_1 and R positive constants (Biot, 1941). We remark that Biot's contribution includes coupling between u and ϑ an we stress again that, contrarily to what is customarily done in classical continuum poroelasticity, the Biot's contribution does not encode the energy part due to interstitial fluid compression. We now discuss the peridynamic (in the sense given by Piola, see dell'Isola et al (2015a)) contribution in Lagrangian form ψ_{PERIDYN} in (3.7). In Eulerian form, the energy stored within the body due to fluid compression is assumed to be

$$\psi_{\text{PERIDYN}} = \frac{1}{2}\beta \int_{\mathcal{B}} \hat{\rho}_{F,C}^2\, \xi_{F,C}\, \mathrm{d}x, \tag{3.12}$$

with $\beta > 0$ being the fluid resistance to compression and the differential $\mathrm{d}V_F = \xi_{F,C}\, \mathrm{d}x$ indicates that integration is taken with respect to the fluid volume. Assuming $\hat{\rho}_{F,C}$ to be uniform over $\mathcal{B}$, and this is reasonable in a quasi-static framework, we have

$$\psi_{\text{PERIDYN}} = \frac{1}{2}\beta \hat{\rho}_{F,C}^2 \int_{\mathcal{B}} \xi_{F,C}\, \mathrm{d}x. \tag{3.13}$$

We now want to transform the integration over the (unknown) deformed shape $\mathcal{B}$ in (3.13) into an integration over the reference shape $\mathcal{B}_0$, i.e. we want to derive ψ_{PERIDYN} in Lagrangian form. To this goal, we perform the change of variable $x = \chi(X)$. We have that $\mathrm{d}x = \det(F)\, \mathrm{d}X + o(\mathrm{d}X)$, with $F = \nabla\chi = I + \nabla u$. Reminding that

$$\det(I + \varepsilon A) = 1 + \varepsilon\, \mathrm{tr}(A) + o(\varepsilon) \tag{3.14}$$

$$\det(I + A) = 1 + \mathrm{tr}(A) + o(A), \tag{3.15}$$

we have $\det(F) = 1 + \mathrm{tr}(\nabla u) + o(\nabla u)$. Since we are working under the small strain hypothesis, observing that $\mathrm{tr}(A) = \mathrm{tr}(\mathrm{Sym}A)$, and neglecting higher order contributions, we have $\det(F) = 1 + \mathrm{tr}(E)$. The volume occupied by the fluid phase in the current configuration is

$$V_F = \int_{\mathcal{B}} \xi_{F,C}\, \mathrm{d}x = \int_{\mathcal{B}_0} \xi_{F,C}^{\mathcal{L}}\, (1 + \mathrm{tr}(E))\, \mathrm{d}X. \tag{3.16}$$

The energy stored within the body due to fluid compression reads thus in Lagrangian form as

$$\psi_{\text{PERIDYN}} = \frac{\beta M_F^2}{2} \frac{1}{\int_{\mathcal{B}_0} \xi_{F,C}^{\mathcal{L}}\, (1 + \mathrm{tr}(E))\, \mathrm{d}X}. \tag{3.17}$$

Of course, we have that

$$\begin{aligned}
&\psi_{\text{PERIDYN}} = \frac{\beta M_F^2}{2} \frac{1}{\int_{\mathcal{B}_0} \xi_{F,C}^{\mathcal{L}} (1 + \mathrm{tr}(E))\, \mathrm{d}X} \frac{\int_{\mathcal{B}} \xi_{F,C}\, \mathrm{d}x}{V_F} = \\
&\frac{1}{V_F} \int_{\mathcal{B}} \frac{\beta M_F^2}{2} \frac{1}{\int_{\mathcal{B}_0} (\xi_{F,R} + \vartheta)(1 + \mathrm{tr}(E))\, \mathrm{d}X}\, \mathrm{d}x = \\
&\frac{1}{\int_{\mathcal{B}_0} (\xi_{F,R} + \vartheta)(1 + \mathrm{tr}(E))\, \mathrm{d}X} \int_{\mathcal{B}_0} \frac{\beta M_F^2}{2} \frac{\xi_{F,C}^{\mathcal{L}} (1 + \mathrm{tr}(E))}{\int_{\mathcal{B}_0} (\xi_{F,R} + \vartheta)(1 + \mathrm{tr}(E))\, \mathrm{d}X} \mathrm{d}X = \\
&\int_{\mathcal{B}_0} \frac{\beta M_F^2}{2} \frac{(\xi_{F,R} + \vartheta)(1 + \mathrm{tr}(E))}{\left[\int_{\mathcal{B}_0} (\xi_{F,R} + \vartheta)(1 + \mathrm{tr}(E))\, \mathrm{d}X\right]^2}\, \mathrm{d}X
\end{aligned} \tag{3.18}$$

where $\xi_{F,C}^{\mathcal{L}} = (\xi_{F,R} + \vartheta)$ has been used. Therefore, the Lagrangian density associated to ψ_{PERIDYN} reads as

$$\frac{\beta M_F^2}{2} \frac{(\xi_{F,R} + \vartheta)\,(1 + \text{tr}(E))}{\left[\int_{\mathcal{B}_0} (\xi_{F,R} + \vartheta)\,(1 + \text{tr}(E))\,\text{d}X\right]^2}. \tag{3.19}$$

We notice that no spatial derivatives of the additional kinematic parameter ϑ appear in the first gradient (with respect to displacement) poroelasticity strain energy ψ_{POR}; hence, the prescription of arbitrary boundary conditions for the porosity field does not yield in general the minimization of the mechanical energy ψ a well-posed problem. Furthermore, we remark that non-locality is given by the peridynamic contribution ψ_{PERIDYN} and not by the dependence of the internal stored energy upon, e.g., higher gradients of the displacement and/or of the change of porosity. Positive definiteness of the isotropic strain energy density of the solid bone-graft mixture is ensured if $\lambda + \mu > 0$ and $\lambda - \mu > 0$, where λ is the effective bone-graft first Lamé parameter and μ is the effective bone-graft shear modulus. Finally, we observe that, following our assumptions, the strain energy is such that remodeling, i.e. a change in the densities of bone tissue and bio-resorbable material in the reference configuration, cannot induce any (local) mechanical anisotropy (for more details see Allena and Cluzel, 2018; Cluzel and Allena, 2018).

3.3.3 Mechanical Stimulus, Bone Remodeling and Graft Resorption

Let $\rho_{OC,R}$ be the Lagrangian density of Osteocytes in the reference configuration. It is assumed to be proportional to the bone density in the reference configuration. Nevertheless, in the literature it is possible to find approaches assuming that the time evolution of the Lagrangian density of Osteocytes in the reference configuration, together with those of Osteoblasts and Osteoclasts, is governed by a distributed cellular population evolution model (Lekszycki and dell'Isola, 2012; George et al, 2018b,c). The Lagrangian mechanical stimulus is defined as

$$S(X,t) = \int_{\mathcal{B}_0} \left[\psi(Y,t)\rho_{OC,R}(Y,t)\, e^{-\frac{(X-Y)^2}{2D^2}}\, \text{d}Y\right] - S_0 \tag{3.20}$$

i.e. it is the 2D Gaussian convolution of the product $\psi\ \rho_{OC,R}$. We remark that the 2D Gaussian $\sim e^{-\frac{(X-Y)^2}{2D^2}}$ has mean X and standard deviation D (variance D^2) and, thus, D is a measure of the circular influence range, since the Gaussian is de facto vanishing at a distance from the mean X greater than three times the standard deviation. We further remark that stimulus is the (spatially) shifted smoothed product $\psi\ \rho_{OC,R}$, which is the Lagrangian strain energy density weighted by the Lagrangian Osteocytes density in the reference configuration; this entails that a non-zero strain

energy density in a sufficiently close neighborhood of a point does not necessarily imply a non-zero stimulus in that point, as in that neighborhood there might be no mechanosensors. Finally, it is worth to be noticed that in the literature (Beaupré et al, 1990; Giorgio et al, 2016) it possible to find a slight variation of the definition of stimulus employed herein, by taking into account a 'dead-zone'

$$S(X,t) = \begin{cases} \tilde{S}(X,t) - S_u & \text{if } \tilde{S}(X,t) \geq S_u \\ \tilde{S}(X,t) - S_d & \text{if } \tilde{S}(X,t) \leq S_d \\ 0 & \text{if } S_d < \tilde{S}(X,t) < S_u \end{cases} \tag{3.21}$$

with

$$\tilde{S}(X,t) = \int_{\mathcal{B}_0} \psi(Y,t)\rho_{OC,R}(Y,t)\, e^{-\frac{(X-Y)^2}{2D^2}}\, \mathrm{d}Y. \tag{3.22}$$

The evolution of graft density due to resorption and of bone density due to formation and resorption is described, for each X, by means of a system of ordinary differential equations

$$\begin{cases} \dot{\rho}_{M,R}(X,t) & = A_M(S)\, H(\xi^{\mathcal{L}}_{F,C}) \\ \dot{\rho}_{B,R}(X,t) & = A_B(S)\, H(\xi^{\mathcal{L}}_{F,C}) \\ \rho_{M,R}(X,0) & = \rho_{M0}(X) \\ \rho_{B,R}(X,0) & = \rho_{B0}(X) \end{cases} \tag{3.23}$$

with

$$H(y) = k\, y(1-y), \qquad \text{with } y \in [0,1] \tag{3.24}$$

$$A_M(S) = \begin{cases} 0 & \text{if } S \geq 0 \\ r_M S & \text{if } S < 0, \end{cases} \tag{3.25}$$

$$A_M(S) = \begin{cases} s_B S & \text{if } S \geq 0 \\ r_B S & \text{if } S < 0, \end{cases} \tag{3.26}$$

and k, r_M, r_B, $s_B \geq 0$. We remark that the function $H(\xi^{\mathcal{L}}_{F,R}) = k\xi^{\mathcal{L}}_{F,R}(1-\xi^{\mathcal{L}}_{F,R})$, a concave symmetric parabola with maximum value $k/4$ attained in $\xi^{\mathcal{L}}_{F,R} = 1/2$ and intersecting the abscissa $H = 0$ in $\xi^{\mathcal{L}}_{F,R} = 0$ and $\xi^{\mathcal{L}}_{F,R} = 1$, accounts for the fact that if the porosity is too low, then living cells will not be able to efficiently resorb the bio-material, neither to form new bone tissue, as the available space will not allow for the activity of a sufficiently large number of actor cells. If the porosity, on the other hand, is too large, then there is not enough solid-phase on which actor cells may deposit, and remodeling will not occur quickly enough. For the sake of simplicity, we set $k = 4$.

3.4 Solution Algorithm and Qualitative Results for Tensile Test

Dimensionless parameters employed for numerical simulations are shown in Tab. 3.1. Specifically, we consider a rectangular sample whose sides are in the ratio 1:3.

The notation $\langle \psi', \delta u \rangle$ denotes the functional derivative of ψ in Eq. (3.6) in the direction δu (displacement variation). For a fixed time instant and corresponding (given) external bulk and surface forces b^{ext}, equation $\langle \psi, \delta u \rangle = 0 \; \forall \delta u$— which corresponds to the so-called weak form— is solved by means of standard finite element techniques included within the weak form package of the commercial software COMSOL Multiphysics$^{\text{TM}}$. From such a computation—$\rho_{B,R}$ and $\rho_{M,R}$ at previous time step are used to retrieve the effective bone-graft Young's modulus—we get the displacement u and change of porosity at time t. Such displacement and $\rho_{OC,R}$—obtained by assuming it to be proportional by a factor K to $\rho_{B,R}$ at the previous time step—are plugged within the Lagrangian mechanical stimulus defined in Eq. (3.20). The so-found Lagrangian mechanical stimulus is inserted with the change of porosity retrieved from the weak form solution in Eq. (3.23) in order to compute $\rho_{B,R}$ and $\rho_{M,R}$ at the current time step. Such values are then used to compute the effective Young modulus to be plugged in the weak form equation at the next time step.

In Fig. 3.3 a block diagram representation of the solution algorithm employed is shown, while a graphical depiction of the test problem is presented in Fig. 3.4. A rectangular slab formed by a rectangular central graft inclusion in bone tissue matrix is subject to a tensile test. In Fig. 3.5, a zoomed detail for the test problem is shown. At the interface between the two phases we consider a spring foundation for both kinematics variables u and ϑ, and a contribution

$$\int_{\partial G} \left[K_u \|u^+ - u^-\|^2 + K_\vartheta \|\vartheta^+ - \vartheta^-\|^2 \right] \mathrm{d}X \tag{3.27}$$

is added to the strain energy. In Fig. 3.6, the evolution in time of minimum graft density (blue), $\min \rho_{M,R}$, and maximum bone tissue density (green), $\max \rho_{B,R}$, over the inclusion zone are shown. Clearly, as time progresses, the graft is resorbed (i.e. the blue curve is monotonously non-increasing) and new bone is formed (i.e. the green curve is monotonously non-decreasing). In Fig. 3.7 the evolution in time of the stimulus S for some relevant time instants is reported. Time increases from left

Table 3.1 Material coefficients in non-dimensional form. Tilde denotes dimensionless quantities.

$\tilde{Y}_B$	$\tilde{Y}_M$	$\tilde{s}_B$	$\tilde{r}_B$	$\tilde{r}_M$
1	1.2	5×10^{8}	5×10^{8}	5×10^{8}
$\tilde{\rho}_{B0} = \tilde{\rho}_{M0}$	$\beta_B = \beta_M$	$\tilde{D}$	K_u	K_ϑ
0.5	2	0.9	0.1	0.1
$\tilde{H}_1$	$\tilde{R}$	$\beta \tilde{M}_F{}^2$	$\tilde{S}_d$	$\tilde{S}_u$
0.8	0.4	1.0×10^{-4}	1.30×10^{-6}	1.30×10^{-6}

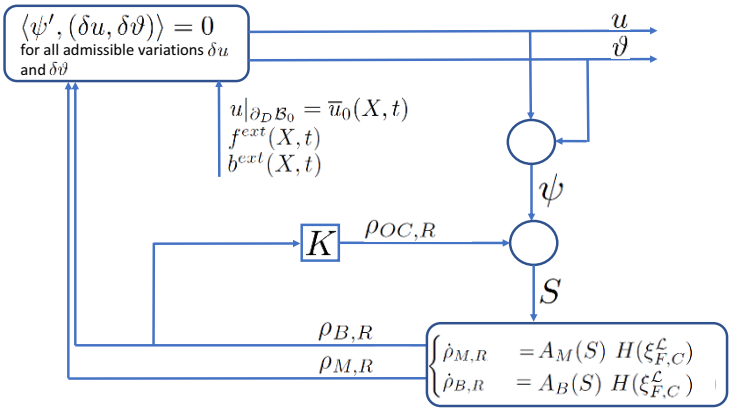

Fig. 3.3 Feedback loop schematic for model solving.

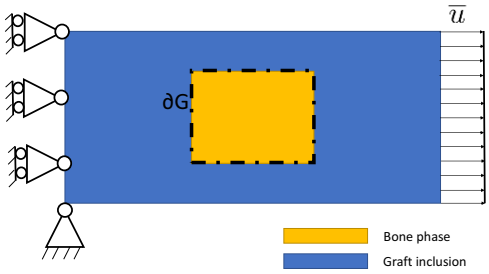

Fig. 3.4 Graphical depiction of the test problem. A rectangular slab formed by a rectangular central graft inclusion in bone tissue matrix is subject to a tensile test.

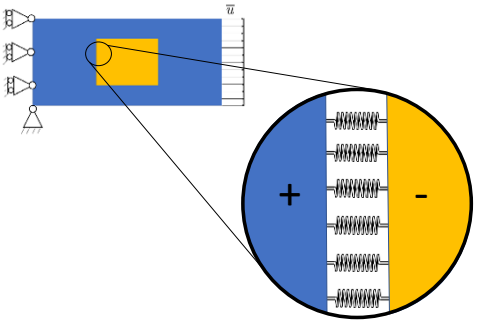

Fig. 3.5 Zoomed detail for the test problem. At the interface between the two phases there is a spring foundation for the variables u and ϑ.

to right and from up to down. As time progresses, the stimulus peaks on the left and on the right of the specimen shift toward the center, and eventually coalesce. The evolution in time of density of Osteocytes $\rho_{OC,R}$ for some relevant time instants is shown in Fig. 3.8. Time increases from left to right and from up to down. Following the feedback behaviour of bone physiology, Osteocytes colonize the graft

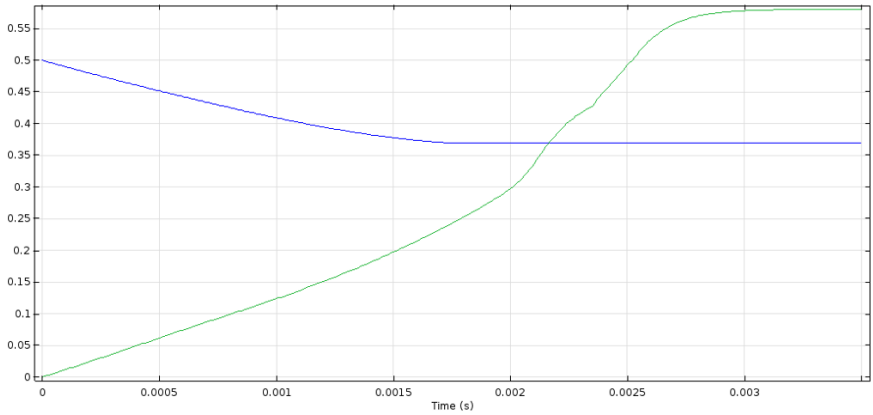

Fig. 3.6 Evolution in time of minimum graft density, $\min \rho_{M,R}$ (blue), and maximum bone tissue density (green), $\max \rho_{B,R}$, over the inclusion zone.

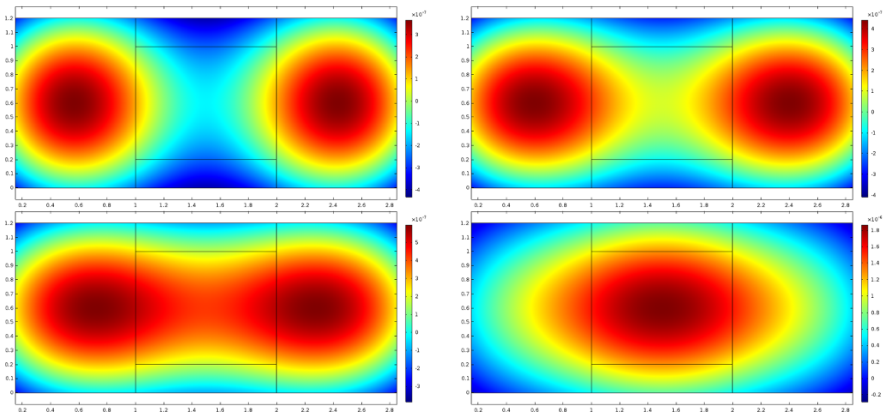

Fig. 3.7 Evolution in time of stimulus for some relevant time instants. Time increases from left to right and from up to down.

gradually, until the inclusion is uniformly saturated by them. The evolution in time of bone tissue density $\rho_{B,R}$ for some relevant time instants is reported as well in Figs. 3.9 and 3.10. Time increases from left to right and from up to down. Finally, evolution in time of the graft density $\rho_{M,R}$ for some relevant time instants is presented in Fig. 3.11. Time increases from left to right and from up to down. Therefore, from Fig. 3.6 it is clear that, as time progresses, the graft is resorbed (i.e. the blue curve is monotonously non-increasing) and new bone is formed (i.e. the green curve is monotonously non-decreasing). Stationary state is reached as both curves are asymptotically approaching limit values.

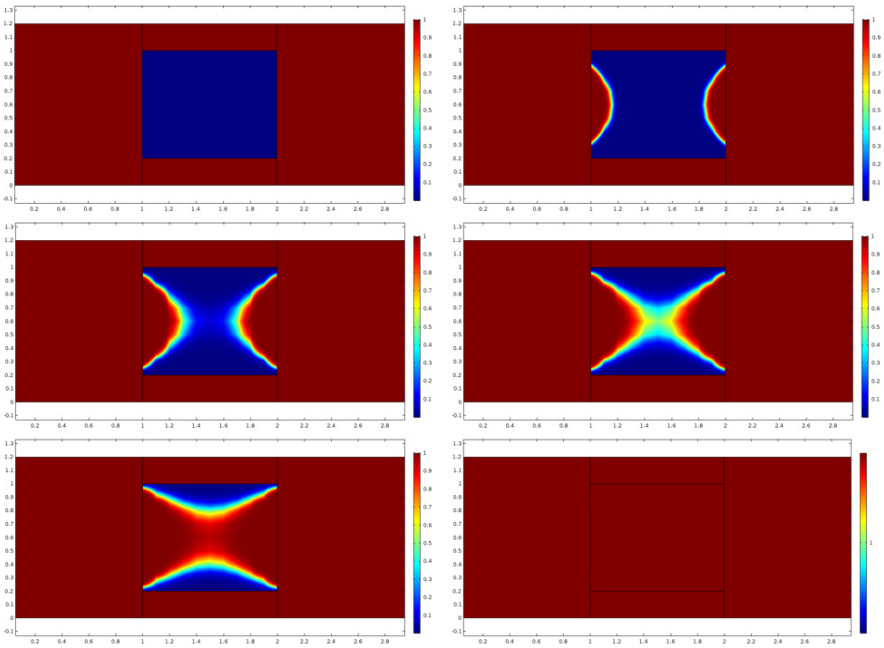

Fig. 3.8 Evolution in time of density of Osteocytes for some relevant time instants. Time increases from left to right and from up to down.

3.5 Conclusion and Outlooks

In this paper, in the framework of poroelasticity, we addressed the study of the interplay between bone remodeling and graft resorption under loading conditions. Aiming at enhancing the modeling proposed in past literature, we considered a physically motivated dedicated strain energy contribution due to the presence of saturating fluid in the interconnected pores, which has some compression resistance. In past literature, the Biot's contribution is not single targeted and includes also, but not only, the effect due to the possible presence of saturating fluid. The classical Biot's strain energy contribution, which is quadratic in the porosity change, is not physically motivated when dealing with the presence of interstitial fluid, and account for the presence of fluid exhibiting resistance to compression must be given in this framework through the 'effective' resistance to the change of porosity. The outlooks of the paper are the following. A parameter estimation from experiments would be useful to allow quantitative (not just qualitative) predictions. Furthermore, the model could be suitably adapted in order to take into account Turner's rules for bone adaptation: (1) remodeling it is driven by dynamic, rather than static, loading; (2) only a short duration of mechanical loading is necessary to initiate an adaptive response; (3) bone cells accommodate to a customary mechanical loading en-

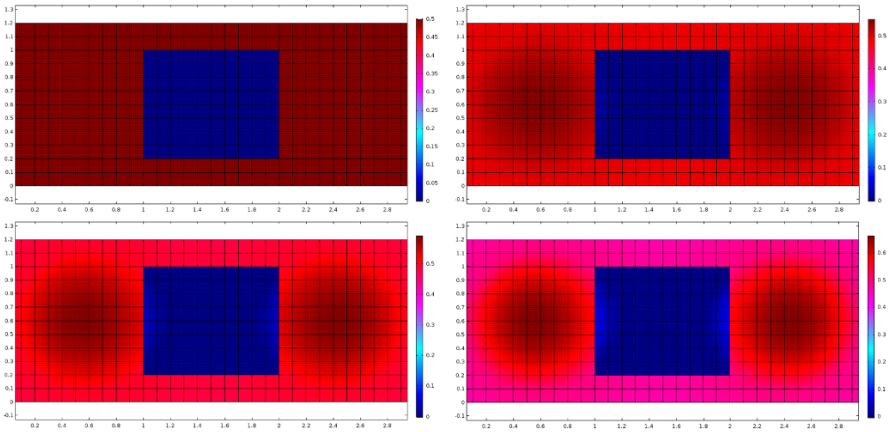

Fig. 3.9 Evolution in time of bone tissue density for some relevant time instants. Time increases from left to right and from up to down.

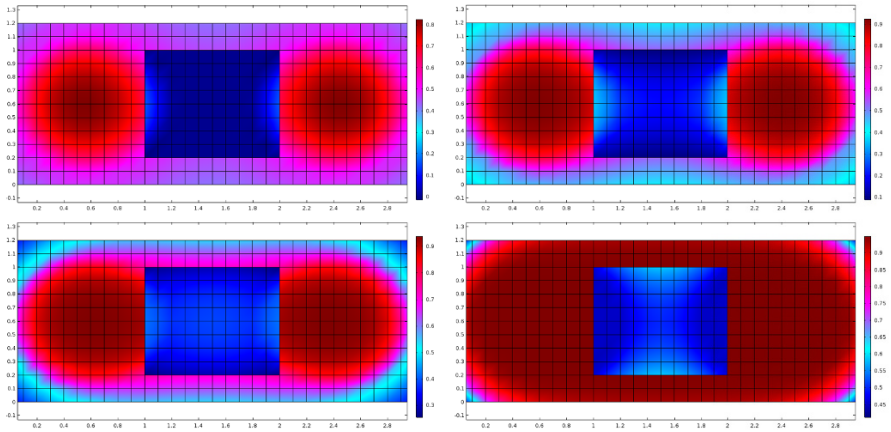

Fig. 3.10 Evolution in time of bone tissue density for some relevant time instants. Time increases from left to right and from up to down.

vironment, making them less responsive to routine loading signals. For example, Turner's rule could be indirectly taken into account by including dissipation. Furthermore, it has to be remarked that, while in this paper a macroscopic continuum model has been formulated directly, a homogenization procedure starting from discrete/continuum descriptions of the phenomena occurring at smaller length scales could give a better insight into the results obtained at the macro-level. In this regard, many procedures, like coarse-graining, hydrodynamical limits (De Masi et al, 2015; De Masi and Olla, 2015; Carinci et al, 2014b,a) for many-particle systems, and computational homogenization (Chatzigeorgiou et al, 2014; Saeb et al, 2016;

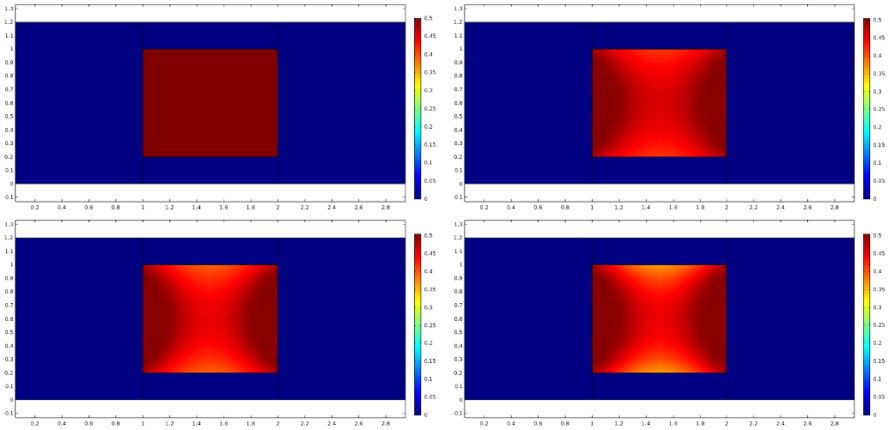

Fig. 3.11 Evolution in time of graft density for some relevant time instants. Time increases from left to right and from up to down.

Javili et al, 2013), are being employed in literature, and they deserve to be better understood.

References

Abali BE, Müller WH, Eremeyev VA (2015) Strain gradient elasticity with geometric nonlinearities and its computational evaluation. Mechanics of Advanced Materials and Modern Processes 1(1):4

Abali BE, Müller WH, dell'Isola F (2017) Theory and computation of higher gradient elasticity theories based on action principles. Archive of Applied Mechanics pp 1–16

Abbas IA, Abdalla AEN, Alzahrani FS, Spagnuolo M (2016) Wave propagation in a generalized thermoelastic plate using eigenvalue approach. Journal of Thermal Stresses 39(11):1367–1377

Abd-alla Aen, Alshaikh F, Del Vescovo D, Spagnuolo M (2017) Plane waves and eigenfrequency study in a transversely isotropic magneto-thermoelastic medium under the effect of a constant angular velocity. Journal of Thermal Stresses 40(9):1079–1092

Abd-alladan AenN, Hamdan AM, Almarashi AA, Battista A (2017) The mathematical modeling for bulk acoustic wave propagation velocities in transversely isotropic piezoelectric materials. Mathematics and Mechanics of Solids 22(4):823–836

Abdoul-Anziz H, Seppecher P (2018) Strain gradient and generalized continua obtained by homogenizing frame lattices. Mathematics and mechanics of complex systems 6(3):213–250

Alibert JJ, Seppecher P, dell'Isola F (2003) Truss modular beams with deformation energy depending on higher displacement gradients. Mathematics and Mechanics of Solids 8(1):51–73

Allena R, Cluzel C (2018) Heterogeneous directions of orthotropy in three-dimensional structures: finite element description based on diffusion equations. Mathematics and Mechanics of Complex Systems 6(4):339–351

Altenbach H, Eremeyev V (2009) On the linear theory of micropolar plates. ZAMM-Journal of Applied Mathematics and Mechanics/Zeitschrift für Angewandte Mathematik und Mechanik 89(4):242–256

Altenbach H, Eremeyev V (2015) On the constitutive equations of viscoelastic micropolar plates and shells of differential type. Mathematics and Mechanics of Complex Systems 3(3):273–283

Altenbach J, Altenbach H, Eremeyev VA (2010) On generalized cosserat-type theories of plates and shells: a short review and bibliography. Archive of Applied Mechanics 80(1):73–92

Andreaus U, Placidi L, Rega G (2010) Numerical simulation of the soft contact dynamics of an impacting bilinear oscillator. Communications in Nonlinear Science and Numerical Simulation 15(9):2603–2616

Andreaus U, Spagnuolo M, Lekszycki T, Eugster SR (2018) A Ritz approach for the static analysis of planar pantographic structures modeled with nonlinear Euler–Bernoulli beams. Continuum Mechanics and Thermodynamics pp 1–21

Auffray N, dell'Isola F, Eremeyev V, Madeo A, Rosi G (2015) Analytical continuum mechanics à la Hamilton–Piola least action principle for second gradient continua and capillary fluids. Mathematics and Mechanics of Solids 20(4):375–417

Battista A, Cardillo C, Del Vescovo D, Rizzi N, Turco E (2015) Frequency shifts induced by large deformations in planar pantographic continua. Nanomechanics Science and Technology: An International Journal 6(2)

Battista A, Del Vescovo D, Rizzi NL, Turco E (2017a) Frequency shifts in natural vibrations in pantographic metamaterials under biaxial tests. Technische Mechanik 37(1):1–17

Battista A, Rosa L, dell'Erba R, Greco L (2017b) Numerical investigation of a particle system compared with first and second gradient continua: Deformation and fracture phenomena. Mathematics and Mechanics of Solids 22(11):2120–2134

Beaupré GS, Orr TE, Carter DR (1990) An approach for time-dependent bone modeling and remodeling—theoretical development. Journal of Orthopaedic Research 8(5):651–661

Berezovski A, Yildizdag ME, Scerrato D (2018) On the wave dispersion in microstructured solids. Continuum Mechanics and Thermodynamics doi: 10.1007/s00161-018-0683-1:1–20

Bertram A, Glüge R (2016) Gradient materials with internal constraints. Mathematics and Mechanics of Complex Systems 4(1):1–15

Biot MA (1941) General theory of three-dimensional consolidation. Journal of applied physics 12(2):155–164

Camar-Eddine M, Seppecher P (2001) Non-local interactions resulting from the homogenization of a linear diffusive medium. Comptes Rendus de l'Academie des Sciences Series I Mathematics 332(5):485–490

Carinci G, De Masi A, Giardinà C, Presutti E (2014a) Hydrodynamic limit in a particle system with topological interactions. Arabian Journal of Mathematics 3(4):381–417

Carinci G, De Masi A, Giardinà C, Presutti E (2014b) Super-hydrodynamic limit in interacting particle systems. Journal of Statistical Physics 155(5):867–887

Chatzigeorgiou G, Javili A, Steinmann P (2014) Unified magnetomechanical homogenization framework with application to magnetorheological elastomers. Mathematics and Mechanics of Solids 19(2):193–211

Cluzel C, Allena R (2018) A general method for the determination of the local orthotropic directions of heterogeneous materials: application to bone structures using μct images. Mathematics and Mechanics of Complex Systems 6(4):353–367

Coussy O (2004) Poromechanics. John Wiley & Sons

Cuomo M (2017) Forms of the dissipation function for a class of viscoplastic models. Mathematics and Mechanics of Complex Systems 5(3):217–237

Cuomo M, dell'Isola F, Greco L, Rizzi N (2016) First versus second gradient energies for planar sheets with two families of inextensible fibres: Investigation on deformation boundary layers, discontinuities and geometrical instabilities. Composites Part B: Engineering

De Masi A, Olla S (2015) Quasi-static hydrodynamic limits. Journal of Statistical Physics 161(5):1037–1058

De Masi A, Galves A, Löcherbach E, Presutti E (2015) Hydrodynamic limit for interacting neurons. Journal of Statistical Physics 158(4):866–902

dell'Isola F, Seppecher P (1997) Edge contact forces and quasi-balanced power. Meccanica 32(1):33–52

dell'Isola F, Steigmann D (2015) A two-dimensional gradient-elasticity theory for woven fabrics. Journal of Elasticity 118(1):113–125

dell'Isola F, Seppecher P, Madeo A (2012) How contact interactions may depend on the shape of Cauchy cuts in Nth gradient continua: approach "à la D'Alembert". Zeitschrift für angewandte Mathematik und Physik 63(6):1119–1141

dell'Isola F, Andreaus U, Placidi L (2015a) At the origins and in the vanguard of peridynamics, non-local and higher-gradient continuum mechanics: An underestimated and still topical contribution of Gabrio Piola. Mathematics and Mechanics of Solids 20(8):887–928

dell'Isola F, Seppecher P, Della Corte A (2015b) The postulations á la D'Alembert and á la Cauchy for higher gradient continuum theories are equivalent: a review of existing results. Proc R Soc A 471(2183):20150,415

dell'Isola F, Madeo A, Seppecher P (2016) Cauchy tetrahedron argument applied to higher contact interactions. Archive for Rational Mechanics and Analysis 219(3):1305–1341

Di Nino S, D'Annibale F, Luongo A (2017) A simple model for damage analysis of a frame-masonry shear-wall system. International Journal of Solids and Structures 129:119–134

Enakoutsa K, DEl Vescovo D, Scerrato D (2017) Combined polarization field gradient and strain field gradient effects in elastic flexoelectric materials. Mathematics and Mechanics of Solids 22(5):938–951

Engelbrecht J, Berezovski A (2015) Reflections on mathematical models of deformation waves in elastic microstructured solids. Mathematics and Mechanics of Complex Systems 3(1):43–82

Eremeyev VA (2018) On the material symmetry group for micromorphic media with applications to granular materials. Mechanics Research Communications 94:8–12

Eremeyev VA, dell'Isola F, Boutin C, Steigmann D (2018a) Linear pantographic sheets: existence and uniqueness of weak solutions. Journal of Elasticity 132(2):175–196

Eremeyev VA, Rosi G, Naili S (2018b) Comparison of anti-plane surface waves in strain-gradient materials and materials with surface stresses. Mathematics and Mechanics of Solids p 1081286518769960

Eugster SR, Glocker C (2017) On the notion of stress in classical continuum mechanics. Mathematics and Mechanics of Complex Systems p 299

Ferretti M, Piccardo G, Luongo A (2017) Weakly nonlinear dynamics of taut strings traveled by a single moving force. Meccanica 52(13):3087–3099

Franciosi P, Spagnuolo M, Salman OU (2018) Mean green operators of deformable fiber networks embedded in a compliant matrix and property estimates. Continuum Mechanics and Thermodynamics doi: 10.1007/s00161-018-0668-0:1–32

Ganghoffer JF (2012) A contribution to the mechanics and thermodynamics of surface growth. application to bone external remodeling. International Journal of Engineering Science 50(1):166–191

Ganghoffer JF (2016) Spatial and material stress tensors in continuum mechanics of growing solid bodies. Mathematics and Mechanics of Complex Systems 3(4):341–363

George D, Allena R, Remond Y (2018a) Cell nutriments and motility for mechanobiological bone remodeling in the context of orthodontic periodontal ligament deformation. Journal of Cellular Immunotherapy

George D, Allena R, Remond Y (2018b) Integrating molecular and cellular kinetics into a coupled continuum mechanobiological stimulus for bone reconstruction. Continuum Mechanics and Thermodynamics pp 1–16

George D, Allena R, Remond Y (2018c) A multiphysics stimulus for continuum mechanics bone remodeling. Mathematics and Mechanics of Complex Systems 6(4):307–319

Giorgio I, Andreaus U, Scerrato D, dell'Isola F (2016) A visco-poroelastic model of functional adaptation in bones reconstructed with bio-resorbable materials. Biomechanics and modeling in mechanobiology 15(5):1325–1343

Giorgio I, Andreaus U, Scerrato D, Braidotti P (2017) Modeling of a non-local stimulus for bone remodeling process under cyclic load: Application to a dental implant using a bioresorbable porous material. Mathematics and Mechanics of Solids 22(9):1790–1805

Goda I, Ganghoffer JF (2015) 3d plastic collapse and brittle fracture surface models of trabecular bone from asymptotic homogenization method. International Journal of Engineering Science 87:58–82

Goda I, Assidi M, Belouettar S, Ganghoffer JF (2012) A micropolar anisotropic constitutive model of cancellous bone from discrete homogenization. Journal of the mechanical behavior of biomedical materials 16:87–108

Goda I, Assidi M, Ganghoffer JF (2014) A 3D elastic micropolar model of vertebral trabecular bone from lattice homogenization of the bone microstructure. Biomech Model Mechanobiol 13:53–83

Gusev AA, Lurie SA (2017) Symmetry conditions in strain gradient elasticity. Mathematics and Mechanics of Solids 22(4):683–691

Hillsley MV, Frangos JA (1994) Bone tissue engineering: the role of interstitial fluid flow. Biotechnology and bioengineering 43(7):573–581

Javili A, Chatzigeorgiou G, Steinmann P (2013) Computational homogenization in magneto-mechanics. International Journal of Solids and Structures 50(25):4197–4216

Lekszycki T, dell'Isola F (2012) A mixture model with evolving mass densities for describing synthesis and resorption phenomena in bones reconstructed with bio-resorbable materials. ZAMM-Zeitschrift für Angewandte Mathematik und Mechanik 92(6):426–444

Lekszycki T, Bucci S, Del Vescovo D, Turco E, Rizzi NL (2017) A comparison between different approaches for modelling media with viscoelastic properties via optimization analyses. ZAMM-Zeitschrift für Angewandte Mathematik und Mechanik 97(5):515–531

Luongo A, D'Annibale F (2017) Nonlinear hysteretic damping effects on the post-critical behaviour of the visco-elastic beck's beam. Mathematics and Mechanics of Solids 22(6):1347–1365

Madeo A, dell'Isola F, Darve F (2013) A continuum model for deformable, second gradient porous media partially saturated with compressible fluids. Journal of the Mechanics and Physics of Solids 61(11):2196–2211

Misra A, Poorsolhjouy P (2015a) Granular micromechanics model for damage and plasticity of cementitious materials based upon thermomechanics. Mathematics and Mechanics of Solids doi: 10.1177/1081286515576821

Misra A, Poorsolhjouy P (2015b) Identification of higher-order elastic constants for grain assemblies based upon granular micromechanics. Mathematics and Mechanics of Complex Systems 3(3):285–308

Misra A, Singh V (2013) Micromechanical model for viscoelastic materials undergoing damage. Continuum Mechanics and Thermodynamics 25(2-4):343–358

Misra A, Singh V (2015) Thermomechanics-based nonlinear rate-dependent coupled damage-plasticity granular micromechanics model. Continuum Mechanics and Thermodynamics 27(4-5):787

Pagnini LC, Piccardo G (2016) The three-hinged arch as an example of piezomechanic passive controlled structure. Continuum Mechanics and Thermodynamics 28(5):1247–1262

Pideri C, Seppecher P (1997) A second gradient material resulting from the homogenization of an heterogeneous linear elastic medium. Continuum Mechanics and Thermodynamics 9(5):241–257

Pietraszkiewicz W, Eremeyev V (2009) On natural strain measures of the non-linear micropolar continuum. International Journal of Solids and Structures 46(3):774–787

Placidi L (2015) A variational approach for a nonlinear 1-dimensional second gradient continuum damage model. Continuum Mechanics and Thermodynamics 27(4-5):623

Placidi L, dell'Isola F, Ianiro N, Sciarra G (2008) Variational formulation of pre-stressed solid–fluid mixture theory, with an application to wave phenomena. European Journal of Mechanics-A/Solids 27(4):582–606

Placidi L, Greco L, Bucci S, Turco E, Rizzi N (2016) A second gradient formulation for a 2d fabric sheet with inextensible fibres. Zeitschrift für angewandte Mathematik und Physik 67(5)(114)

Placidi L, Barchiesi E, Misra A (2018) A strain gradient variational approach to damage: a comparison with damage gradient models and numerical results. Mathematics and Mechanics of Complex Systems 6(2):77–100

Rinaldi A, Placidi L (2014) A microscale second gradient approximation of the damage parameter of quasi-brittle heterogeneous lattices. ZAMM-Journal of Applied Mathematics and Mechanics/Zeitschrift für Angewandte Mathematik und Mechanik 94(10):862–877

Rosi G, Placidi L, Auffray N (2018) On the validity range of strain-gradient elasticity: a mixed static-dynamic identification procedure. European Journal of Mechanics-A/Solids 69:179–191

Saeb S, Steinmann P, Javili A (2016) Aspects of computational homogenization at finite deformations: A unifying review from Reuss' to Voigt's bound. Applied Mechanics Reviews 68(5):050,801

Sciarra G, dell'Isola F, Coussy O (2007) Second gradient poromechanics. International Journal of Solids and Structures 44(20):6607–6629

Seppecher P (1993) Equilibrium of a Cahn-Hilliard fluid on a wall: influence of the wetting properties of the fluid upon the stability of a thin liquid film. European journal of mechanics series B fluids 12:69–69

Seppecher P (2000) Second-gradient theory: application to Cahn-Hilliard fluids. In: Continuum thermomechanics, Springer, pp 379–388

Seppecher P, Alibert JJ, dell'Isola F (2011) Linear elastic trusses leading to continua with exotic mechanical interactions. In: Journal of Physics: Conference Series, IOP Publishing, vol 319, p 012018

Shirani M, Andani MT, Kadkhodaei M, Elahinia M (2017) Effect of loading history on phase transition and martensitic detwinning in shape memory alloys: Limitations of current approaches and development of a 1d constitutive model. Journal of Alloys and Compounds 729:390–406

Spagnuolo M, Andreaus U (2018) A targeted review on large deformations of planar elastic beams: extensibility, distributed loads, buckling and post-buckling. Mathematics and Mechanics of Solids p 1081286517737000

Spagnuolo M, Barcz K, Pfaff A, dell'Isola F, Franciosi P (2017) Qualitative pivot damage analysis in aluminum printed pantographic sheets: numerics and experiments. Mechanics Research Communications

Spingarn C, Wagner D, Remond Y, George D (2018) Theoretical numerical modeling of the oxygen diffusion effects within the periodontal ligament for orthodontic tooth displacement. Journal of Cellular Immunotherapy

Steigmann D, Agrawal A (2016) Electromechanics of polarized lipid bilayers. Mathematics and Mechanics of Complex Systems 4(1):31–54

Wilmanski K (1998) A thermodynamic model of compressible porous materials with the balance equation of porosity. Transport in Porous Media 32(1):21–47